Trans. Phenom. Nano Micro Scales, 5(1): 30-43, Winter - Spring 2017
DOI: 10.7508/tpnms.2017.01.004

ORIGINAL RESEARCH PAPER

Mixed convection fluid flow and heat transfer and optimal distribution of discrete heat sources location in a cavity filled with nanofluid

A. A Abbasian Arani [1], M. Abbaszadeh [,1], A. Ardeshiri [1]*

[1]*Mechanical Engineering Department, University of Kashan, Kashan, I. R.Iran*

Received 19 August 2015; revised 21 October 2015; accepted 21 November 2015; available online 24 December 2016

ABSTRACT: Mixed convection fluid flow and heat transfer of water-Al_2O_3 nanofluid inside a lid-driven square cavity has been examined numerically in order to find the optimal distribution of discrete heat sources on the wall of a cavity. The effects of different heat source length, Richardson number and Grashof number on optimal heat source location has been investigated. Moreover, the average Nusselt number on the heat source for two models of nanofluid, constant properties and variable properties, are compared. The obtained results showed that by decreasing the Richardson number and increasing the Grashof number, heat transfer rate decreases. Also by reducing the Richardson number, optimal heat source location move to the top of the wall and with augmentation of Richardson number, heat source optimal location move to the middle of the wall. Furthermore, the overall heat transfer increases by increasing nanoparticles volume fraction. Moreover, it was found that for two different models of nanofluids and in Ri=1, the values of the average Nusselt number are close together.

KEYWORDS: *Mixed convection; Nanofluids; Heat sources; Optimization*

Introduction

Fluid flow and heat transfer in a cavity which is driven by buoyancy and shear force are encountered in a variety of thermal engineering applications [1–2]. Interaction of buoyancy force due to temperature gradient and forced convection due to shear forces is a complex phenomenon in mixed convection flow and heat transfer. Numerous researches on this type of problem including the single or double lid-driven cavity flow and heat transfer involving different cavity configurations, various fluids and imposed temperature gradients have been published in the last two decades [3-9]. For example, Sharif [10] studied laminar mixed convection in a shallow inclined cavity where the top wall is hot and the bottom wall is cool. He demonstrated that the average Nusselt number increases by increasing the cavity inclination angle for forced convection-dominated regime (Ri=0.1) while it increases more rapidly for natural convection-dominated regime (Ri=10).

Tiwari and Das [11] numerically investigated the mixed convection heat transfer and fluid flow of Cu–water nanofluid in a square cavity with top and bottom insulated walls and differentially-heated moving sidewalls. They found that when the Ri=1, the average Nusselt number increases substantially with augmentation of the volume fraction of the nanoparticles. Muthtamilselvan et al. [12] numerically scrutinized the mixed convection flow and heat transfer of Cu–water nanofluid in a lid-driven rectangular enclosure. The sidewalls of the enclosure were adiabatic while the horizontal walls were kept at constant temperatures and the top wall moved at a constant velocity. Arefmanesh and Mahmoodi [13] performed a numerical study to examine the effects of uncertainties of viscosity models for the Al_2O_3–water nanofluid on mixed convection in a square cavity with cold left, right, and top walls and hot bottom wall. Their results showed that the average Nusselt number of the hot wall increases by increasing the volume fraction of nanoparticles for both viscosity models which are used. Kandaswamy et al. [14] conducted a numerical study on buoyancy-driven convection in a cavity with partially thermally active vertical walls. They obtained that heat transfer rate is increased when the heating location is at middle of the hot wall. Mahmoodi [15] investigated mixed convection flow of water-Al_2O_3 nanofluid in a rectangular cavity. He observed that the heat transfer rate increases due to existence of nanoparticles in the base fluid for all range of considered Richardson number. Sebdani et al. [16] conducted a numerical simulation to investigate the effect of nanofluid variable properties on mixed convection in a square cavity with moving cold side walls and a constant temperature heater on the bottom wall. Their results showed that the heat transfer of the nanofluid could be either enhanced or alleviated with respect to the base fluid which is depending on the Reynolds number and Rayleigh number. Amiri et al. [17] provided a numerical simulation of combined thermal and mass transport in a square lid-driven cavity.

*Corresponding Author Email: *abbaszadeh.mahmoud@gmail.com*
Tel.: 09378056718; Note. This manuscript was submitted on August 19, 2015; approved on October 21, 2016; published online December 24, 2016.

Nomenclature

C	Overall heat transfer	u	velocity component in the direction of x(m/s)
$\bar{D}_0$	Heat source length	v	velocity component in the direction of y(m/s)
c_P	Specific heat at constant pressure(J/kgK)	U	Dimensionless velocity component in the direction of X
F	Buoyancy force$(Kgms^{-2})$	V	Dimensionless velocity component in the direction of Y
g	Acceleration of gravity(m/s^2)		**Greek Symbols**
Gr	Grashof Number	α	Thermal diffusivity(m^2/s)
H	The height of cavity(m)	β	Coefficient of thermal expansion$(1/K)$
K	Conduction heat transfer coefficient(W/mK)	μ	Viscosity(kg/ms)
Nu_{avg}	The average Nusselt number	ν	Kinematic viscosity(m^2/s)
Nu_y	Local Nusselt number	θ	Dimensionless temperature
Ma	Mach number	ρ	Density(kg/m^3)
p	Pressure(N/m^2)	φ	Volume fraction of nanoparticles
p	Dimensionless pressure		**Subscripts**
p_r	Prandtl number	avg	Average
Re	Reynolds number	c	Cold
Ra	Rayleigh number	Opt	Optimum
Ri	Richardson number	f	Fluid
T	Temperatuer(K)	h	Hot
		nf	Nanofluid
		p	Nanoparticle

Their results demonstrated that the heat and mass transfer rates inside the cavity increases for low values of Richardson numbers. The other applications of the mixed convection and also, using nanofluids as an innovative approach to enhance heat transfer can be found in references [18-36]. The convective heat transfer problem and optimal heat sources locations in enclosures have been studied in many literatures due to wide range of engineering applications in such processes. For instance, the thermal performance of electronic packages containing a number of discrete heat sources has been studied extensively. The design problem in electronic packages is to maintain cooling of chips in an effective way to prevent overheating and hot spots. This is achieved generally by effective cooling by natural convection, mixed convection and in certain cases by other means such as heat pipes, and finally by better design. In the latter case, the objective is to maximize heat transfer density so that the maximum temperature specified for safe operation of a chip is not exceeded. Thus, optimum placement of discrete heaters may be required with respect to usual equidistant placement. Muftuoglu and Bilgen [37] determined the optimum position of a discrete heater by maximizing the conductance and then studied heat transfer and volume flow rate with the discrete heater at its optimum position in open cavities by using the finite difference-control volume numerical method. The optimum position of single and multiple chips has been studied in references [38-39]. Recently, Dias and Milanez [40] have used genetic algorithms in order to optimize the heat sources in a cavity. In this paper, a numerical study has been done in order to find the optimal distribution of discrete heat sources on the wall in a lid-driven square cavity filled with nanofluid. The effects of different heat source length values, Richardson number and Grashof number on optimal heat source location has been investigated. Results of flow field and heat transfer simulation in different conditions such as heat source movement, variation of heat sources length, Richardson number, Grashof number, nanoparticles volume fraction have been investigated. Also the average Nusselt number on the heat source for two models of nanofluid, constant properties and variable properties, are compared.

The geometry, governing equations and boundary conditions

In the present study a steady two-dimensional and laminar nanofluid flow inside the cavity is considered. The geometry is shown in Figure 1.

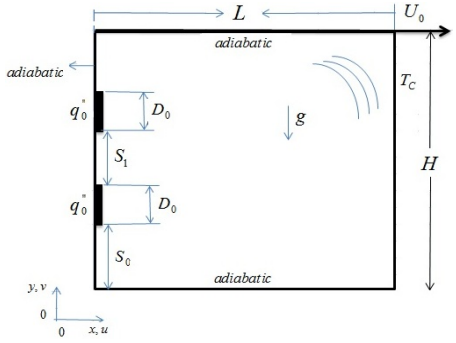

Fig. 1. Schematic diagram of the physical system

Length and height of the cavity are equal (L=H). The top wall is insulated and moves in constant velocity U_0 from

left to right. The right wall is at a constant temperature T_0 and heat sources with constant flux $q_0^{"}$ and D_0 length are on the left insulated wall. The bottom wall is adiabatic. The cavity is filled with water-Al_2O_3 nanofluids. Thermophysical properties of base fluid and particles are presented in Table 1. In addition, viscosity and density is considered vary with temperature and volume fraction. The nanofluid is considered Newtonian and incompressible. The density changes according to Boussinesq approximation [43]. Steady-state continuity, momentum and energy equations in Cartesian coordinates are as follows:

Table 1
Thermophysical properties of water and Al_2O_3 nanoparticles at 25° [44].

Physical Properties	Water	Al_2O_3
$\rho(kg/m^3)$	997.1	3790
cp(J/(kgK))	4197	765
k(W/(mK))	0.613	40
$\beta \times 10^{-5}(1/K)$	21	0.85

$$\frac{\partial u}{\partial x}+\frac{\partial v}{\partial y}=0 \tag{1}$$

$$\rho_{nf}(u\frac{\partial u}{\partial x}+v\frac{\partial v}{\partial y})=-\frac{\partial p}{\partial x}+\frac{\partial}{\partial x}\left(\mu_{nf}\frac{\partial u}{\partial x}\right)+\frac{\partial}{\partial y}\left(\mu_{nf}\frac{\partial v}{\partial y}\right) \tag{2}$$

$$\rho_{nf}(u\frac{\partial u}{\partial x}+v\frac{\partial v}{\partial y})=-\frac{\partial p}{\partial x}+\frac{\partial}{\partial x}\left(\mu_{nf}\frac{\partial u}{\partial x}\right)+\frac{\partial}{\partial y}\left(\mu_{nf}\frac{\partial v}{\partial y}\right)+\left(\rho\beta\right)_{nf}g(T-T_c) \tag{3}$$

$$\left(\rho c_p\right)_{nf}(u\frac{\partial T}{\partial x}+v\frac{\partial T}{\partial y})=-\frac{\partial p}{\partial x}+\frac{\partial}{\partial x}\left(k_{nf}\frac{\partial T}{\partial x}\right)+\frac{\partial}{\partial y}\left(k_{nf}\frac{\partial T}{\partial y}\right) \tag{4}$$

where the density, heat capacity, thermal expansion coefficient, and thermal diffusivity of the nanofluid are as follow[45]:

$$\rho_{nf}=(1-\varphi)\rho_f+\varphi\rho_P \tag{5}$$

$$\left(\rho c_p\right)_{nf}=(1-\varphi)\left(\rho c_p\right)_f+\varphi\left(\rho c_p\right)_p \tag{6}$$

$$\left(\rho\beta\right)_{nf}=(1-\varphi)\left(\rho\beta\right)_f+\varphi\left(\rho\beta\right)_p \tag{7}$$

$$\alpha_{nf}=\frac{k_{nf}}{\left(\rho c_p\right)_{nf}} \tag{8}$$

The effective dynamic viscosity of the water-Al_2O_3 nanofluid is calculated according to the Brinkman model [48] and variable properties Khanafer and Vafai model [42].

$$\mu_{nf}=\frac{\mu_f}{(1-\varphi)^{2.5}} \tag{9}$$

$$(\mu_{nf})_{Al_2O_3}=-0.4491+\frac{28.837}{T}+0.574\varphi_p-0.1634{\varphi_p}^2+23.053\frac{{\varphi_p}^2}{T^2}+0.0132{\varphi_p}^3-2354.735\frac{\varphi_p}{T^3}+23.498\frac{{\varphi_p}^2}{d_p^2}-3.0185\frac{{\varphi_p}^3}{d_p^2} \tag{10}$$

Khanafer and Vafai model [42] is used in a wide range of nanoparticle diameter 13nm ≤ d_p ≤ 131nm, volume fraction 1%≤φ_p≤9% and temperature 20≤T(°C)≤70.

The effective thermal conductivity of the nanofluid is determined using the Maxwell model [41], which is:

$$\frac{k_{eff}}{k_f}=\frac{(k_s+2k_f)-2\varphi(k_f-k_s)}{(k_s+2k_f)+\varphi(k_f-k_s)} \tag{11}$$

$$\left(\frac{k_{nf}}{k_f}\right)_{Al_2O_3}=0.9843+0.398{\varphi_p}^{0.7383}\left(\frac{1}{d_p\,(nm)}\right)^{0.2246}\left(\frac{\mu_{nf}(T)}{\mu_f(T)}\right)^{0.0235}-3.9517\frac{\varphi_p}{T}+34.034\frac{{\varphi_p}^2}{T^3}+32.509\frac{\varphi_p}{T^2} \tag{12}$$

Temperature range, diameter and volume fraction of nanoparticles in equation 12 in 0%≤φ_p≤10%, 20≤T(°C)≤ 70, 11nm≤d_p≤150nm are valid, respectively.

Water dynamic viscosity at different temperatures can be expressed as follows [42]:

$$\mu_f\left(T\right)=2.414\times10^{-5}\times10^{\frac{247.8}{(T-140)}} \tag{13}$$

To convert the governing equations 1–4 into dimension - less form, the following dimensionless parameters are employed:

$$U=\frac{u}{U_0},\ V=\frac{v}{U_0},\ \left(X,Y,\tilde{D}_0,\tilde{S}_i\right)=\frac{\left(x,y,D_0,S_i\right)}{H},\quad \theta_{\max}=\frac{T_{\max}-T_c}{q_0^{"}H/k_f},\ P=\frac{p}{\rho_{nf}U_0^2},\ q^{"}=\frac{k\,(\partial T/\partial x)}{q_0^{"}} \tag{14}$$

The dimensionless forms of the governing equations are:

$$\frac{\partial U}{\partial X}+\frac{\partial V}{\partial Y}=0 \tag{15}$$

$$U\frac{\partial V}{\partial X}+V\frac{\partial U}{\partial Y}=-\frac{\partial P}{\partial X}+\frac{1}{\mathrm{Re}}\frac{1}{\nu_f\rho_{nf}}\left[\frac{\partial}{\partial X}(\mu_{nf}\frac{\partial U}{\partial X})+\frac{\partial}{\partial Y}(\mu_{nf}\frac{\partial U}{\partial Y})\right] \tag{16}$$

$$U\frac{\partial V}{\partial X}+V\frac{\partial V}{\partial Y}=-\frac{\partial P}{\partial Y}+\frac{1}{\mathrm{Re}}\frac{1}{\nu_f\rho_{nf}}\left[\frac{\partial}{\partial X}(\mu_{nf}\frac{\partial V}{\partial X})+\frac{\partial}{\partial Y}(\mu_{nf}\frac{\partial V}{\partial Y})\right]+\frac{(\rho\beta)_{nf}}{\rho_{nf}\beta_f}\frac{Gr}{\mathrm{Re}^2}\theta \tag{17}$$

$$U\frac{\partial \theta}{\partial X}+V\frac{\partial \theta}{\partial Y}=\frac{\alpha_{nf}}{\alpha_f}\frac{1}{k_{nf}}\frac{1}{\mathrm{Pr}\,\mathrm{Re}}\left[\frac{\partial}{\partial X}\left(k_{nf}\frac{\partial \theta}{\partial X}\right)+\frac{\partial}{\partial Y}\left(k_{nf}\frac{\partial \theta}{\partial Y}\right)\right] \tag{18}$$

The Grashof number, the Reynolds number and the Prandtl number are defined as:

$$Gr=\frac{\beta g H^3\left(T_{\max}-T_c\right)}{\upsilon^2},\ \mathrm{Re}=\frac{UH}{\upsilon},\ Pr=\frac{\upsilon}{\alpha} \tag{19}$$

The boundary conditions for the governing equations are:

$$Y=0,\ 0\le X\le L:\quad U=V=0,\ \frac{\partial\theta_{\max}}{\partial Y}=0$$

$$Y=H,\ 0\le X\le L:\quad U=U_0,\ V=0,\ \frac{\partial\theta_{\max}}{\partial Y}=0$$

$$X=0,\ 0\le Y\le S_0:U=V=0,\ \frac{\partial\theta_{\max}}{\partial X}=0 \tag{20}$$

$$X=0,\ \tilde{S}_0\le Y\le\tilde{S}_0+\tilde{D}_0:\quad U=V=0,\ k_{nf}\left(\frac{\partial\theta_{\max}}{\partial X}\right)=q^{"}$$

$$X=0,\ \tilde{S}_0+\tilde{D}_0\le Y\le H:\quad U=V=0,\ \frac{\partial\theta_{\max}}{\partial X}=0$$

The local Nusselt number is calculated by:

$$Nu(s)=\frac{h_{nf}L}{k_f} \tag{21}$$

where the heat transfer coefficient is:

$$h_{nf}=-\frac{k_{nf}\left.\frac{\partial T}{\partial y}\right|_{y=0}}{T_{\max}-T_c} \tag{22}$$

The thermal conductivity is calculated according to the following expression:

$$k_{nf}=-\frac{k_f\left.\frac{\partial T}{\partial y}\right|_{y=0}}{\partial T/\partial x} \tag{23}$$

By substituting equations 22 and 23 into equation 21, the Nusselt number can be written as:

$$Nu(s)=-\frac{k_{nf}}{k_f}\frac{\partial\theta}{\partial Y} \tag{24}$$

By integrating the local Nusselt number along the hot wall, the average Nusselt number is calculated by:

$$Nu_{avg}=\frac{1}{\Delta s}\int_s^{s+\Delta s}Nu(s)\,ds \tag{25}$$

The overall heat transfer inside the enclosure is defined as follows:

$$C=\frac{Q'}{k_f\left(T_{\max}-T_C\right)} \tag{26}$$

$Q^{'}$ is the total heat flux in the cavity and is obtained according to equation 27:

$$Q^{'}=q_0^{"}\times D_0\times N \tag{27}$$

Which N is the number of heat sources and D_0 is the length of heat source.

Numerical simulation

Governing equations are solved numerically using the finite volume method and SIMPLER algorithm. At first a uniform and appropriate grid is coincided to the solution field and then around each node, a control volume is

considered and the governing equations are integrated on each control volume and equations are dismissed and a system of algebraic equations is obtained. For separation convection and diffusion terms the hybrid method is used. In this method the central difference scheme is used for the Peclet numbers with absolute value less than 2 and the upwind scheme is used for the Peclet numbers with absolute value more than 2. In order to achieve the convergence, the under relaxation coefficient is used. It is 0.5 for velocity components and 0.7 for temperature. Convergence criteria for pressure, velocity and temperature is obtained by equation 28, where M and N is the number of grids in the x and y direction and "ζ " represents a variable which is solved. k is number of iterations and the maximum error is 10^{-6}.

$$\text{Error} = \frac{\sum_{i=1}^{M}\sum_{j=1}^{N}\left|\zeta_{i,j}^{k+1} - \zeta_{i,j}^{k}\right|}{\sum_{i=1}^{M}\sum_{j=1}^{N}\left|\zeta_{i,j}^{k+1}\right|} \le 10^{-6} \qquad (28)$$

Grid independency test

Numerical code was tested for grid independence by calculating the average Nusselt number on the heat source surface according to Table 2. It was found that a grid size of 101×121 ensures a grid independent solution in non-uniform mesh.

Table 2
Average Nusselt number for different grids.

Grid size	Average Nusselt number
101×101	654.2
111×101	801.2
101×121	879.2
101×131	907.2

Validation of results

To validate the computer program results, Silva et al. [46] and Sivakumar et al. [47] solution geometry with our program are simulated. The results of the overall heat transfer rates at various locations inside the cavity and the average Nusselt number in Re=100 are compared with their results in Figure 2 and Tables 3.

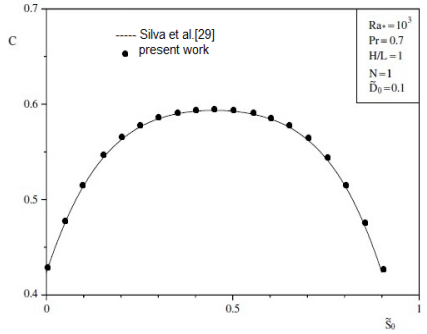

Fig. 2. Overall heat transfer in various locations along the wall

As can be seen for the same conditions, a good agreement exists. Also the small amounts of the numerical difference represent the computer code accuracy which is used.

Table 3
Comparing the average Nusselt number in mixed convection.

Richardson Number	Distance from the heat source to the bottom of the cavity	Average Nusselt Number	
		Reference Results[47]	Present Study
Ri=0.1	ε_2=1.6	3.63	3.71
	ε_2=3.6	5.24	5.30
	ε_2=5.6	5.67	5.74
Ri=1	ε_2=1.6	4.65	4.72
	ε_2=3.6	6.41	6.49
	ε_2=5.6	5.97	6.06
Ri=10	ε_2=1.6	7.91	8.04
	ε_2=3.6	9.04	9.16
	ε_2=5.6	7.48	7.59

Results and discussion

In this section, the results such as the stream lines, the isotherm lines, the average Nusselt number and the overall heat transfer in terms of parameters such as the Richardson number, Grashof number, Reynolds number and volume fraction are presented and discussed. The various conditions are being studied for different Richardson number Ri= 0.1, 1, 4 and 10 and in constant Grashof numbers 10^2, 10^3 and 10^4. In this study, three different heat source lengths (%D_0= 0.05, 0.1, 0.2) are used. Also different volume fraction values have been used to study the effect of the nanoparticles volume fraction on heat transfer. Finally the effect of using nanofluids variable properties and constant properties on average Nusselt number are compared.

Finding the optimal location for one heat source

In Figure 3, the overall heat transfer in term of the distance between the end of the heat source and bottom of the cavity for the dimensionless length 0.1, φ=0.5 and in different Richardson numbers and constant Grashof numbers Gr=10^2 -10^3 is shown.

As can be seen in this figure, the part of the curves which have the peak of C, represents heat source optimal location (%$S_{0.opt}$) which is a unique point for each curves. It should be noted that the overall heat transfer has a direct relation with the heat source maximum temperature. Also the optimal location and the overall heat transfer depend on the Richardson number and the Grashof number.

When the heat source is located at the bottom of the wall, the overall heat transfer is almost independent from the Richardson number. This is due to weak flow strength in the subordinate edge of the cavity that reduces the heat transfer rate in this area. But by increasing the distance

between the heat source and the bottom wall, the difference between the values of C are intensified in different Richardson numbers.

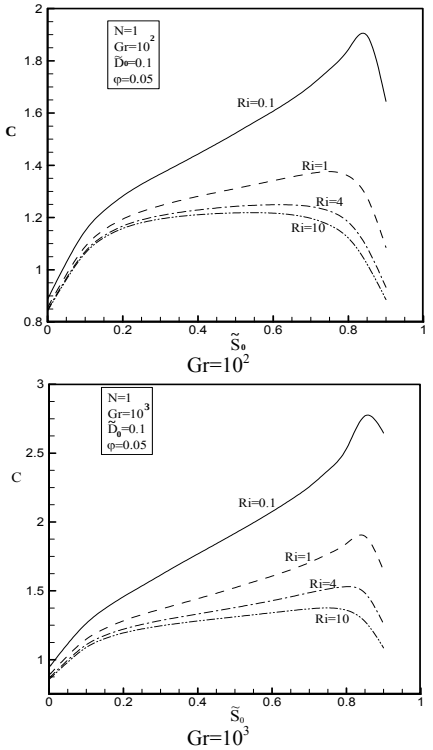

Fig. 3. The overall heat transfer in terms of the distance between the heat source and the bottom wall

As shown in Figure 3, by increasing the Richardson number, force convection reduces and as a result, the heat transfer rate inside the cavity, especially at the upper corners, decreases. Therefore, the heat source optimal location is migrated from the top wall to the middle part of the left wall.

Figure 4 elucidates how the optimum heat source location responds to the Grashof number in addition to Richardson number.

The changes of the optimum heat source location in low Grashof numbers is more than high Grashof numbers as far as the Grashof number is the proportion of the buoyancy force to viscosity force. In general, when the Grashof number increases, the overall heat transfer increases inside the cavity. Thus in low Grashof number the heat source should be transmitted to the middle of the cavity in order to increase heat transfer.

The exact values of the optimal heat source location and maximum overall heat transfer in different Richardson numbers and in constant Grashof number are represented in Table 4. According to these results, the optimal location for high Grashof number is near the top wall and the lid-driven. But in low Grashof number, the optimum location in different Richardson numbers changes.

The changing is near the middle part of the wall up to lid-driven.

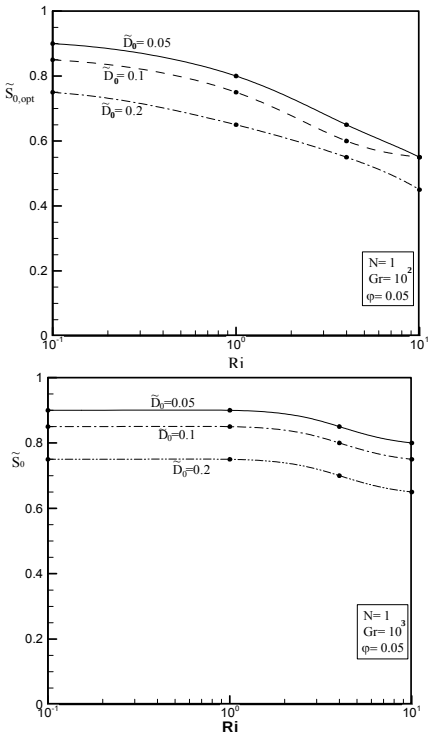

Fig. 4. Distance between the heat source and the bottom wall in terms of Richardson number

Finding the optimal location for two discrete heat sources

In this section, the position of two separate heat sources with equal length and heat flux is optimized. Distance between the first heat source to the bottom wall is $\widetilde{S_0}$ and the distance between the two heat sources is specified by $\widetilde{S_1}$.

As illustrated in Figure 5, in Ri=4, at first the overall heat transfer increases by increasing $\widetilde{S_0}$ and then at the end of the wall decreases. Also when the first heat source approaches to the end of the wall, the second heat source location plays an important role in overall heat transfer rate in which by closing to the lid-driven, a severe decrease in overall heat transfer takes place.

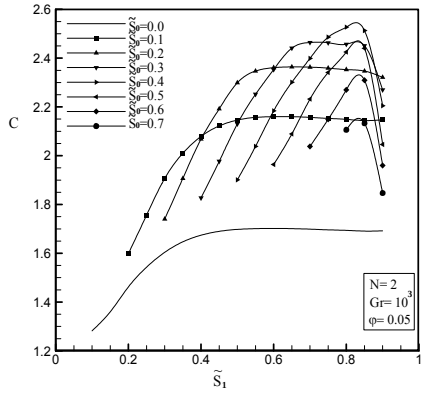

Fig. 5. Overall heat transfer (C) in terms of $\widetilde{S_1}$ for different $\widetilde{S_0}$

The optimal heat sources location $\widetilde{S_0}$ and $\widetilde{S_1}$ in term of Richardson number and in $Gr=10^3$ and $\varphi=0.05$ are indicated in Figure 6. As can be seen for low Richardson number, two heat sources are placed in the upper half of the wall and for high Richardson numbers, optimal heat sources location are placed in middle part of the wall. Figure 7 shows the maximum overall heat transfer for two separate heat sources in different Richardson numbers and in $Gr=10^3$ and $\varphi=0.05$.

It is obvious that the maximum overall heat transfer inside the cavity reduces by increasing the Richardson number.

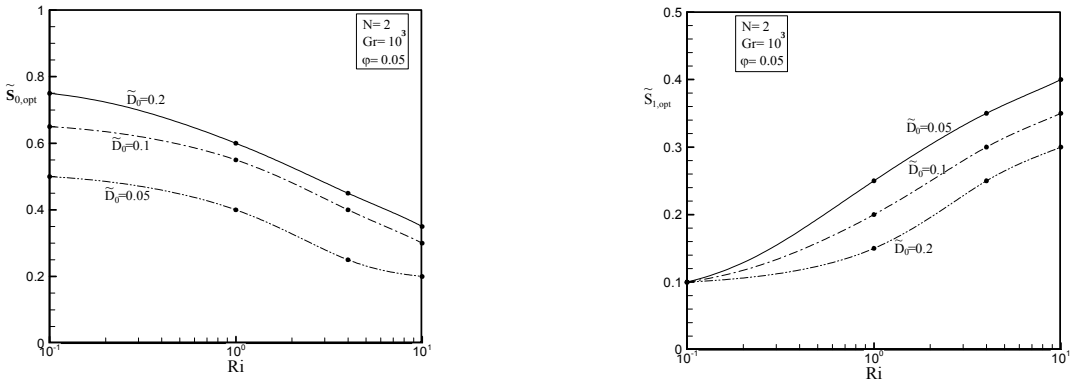

Fig. 6. Optimal location for two separate heat sources in terms of Richardson number in $Gr=10^3$ and $\varphi=0.05$

Table 4

Optimum heat source location ($\%S_{0.opt}$) and maximum overall heat transfer (C_{max}) for different Richardson numbers and constant Grashof numbers.

		Ri=0.1	**Ri=1**	**Ri=4**	**Ri=10**
$Gr=10^2$	$\%D_0=0.05$	$C_{max}=1.367$ $\%S_{0,opt}=0.90$	$C_{max}=1.014$ $\%S_{0,opt}=0.80$	$C_{max}=0.930$ $\%S_{0,opt}=0.65$	$C_{max}=0.911$ $\%S_{0,opt}=0.55$
	$\%D_0=0.1$	$C_{max}=1.896$ $\%S_{0,opt}=0.85$	$C_{max}=1.375$ $\%S_{0,opt}=0.75$	$C_{max}=1.249$ $\%S_{0,opt}=0.60$	$C_{max}=1.218$ $\%S_{0,opt}=0.55$
	$\%D_0=0.2$	$C_{max}=2.608$ $\%S_{0,opt}=0.75$	$C_{max}=1.895$ $\%S_{0,opt}=0.65$	$C_{max}=1.718$ $\%S_{0,opt}=0.55$	$C_{max}=1.671$ $\%S_{0,opt}=0.45$
$Gr=10^3$	$\%D_0=0.05$	$C_{max}=1.965$ $\%S_{0,opt}=0.90$	$C_{max}=1.367$ $\%S_{0,opt}=0.90$	$C_{max}=1.123$ $\%S_{0,opt}=0.85$	$C_{max}=1.014$ $\%S_{0,opt}=0.80$
	$\%D_0=0.1$	$C_{max}=2.771$ $\%S_{0,opt}=0.85$	$C_{max}=1.896$ $\%S_{0,opt}=0.85$	$C_{max}=1.530$ $\%S_{0,opt}=0.80$	$C_{max}=1.375$ $\%S_{0,opt}=0.75$
	$\%D_0=0.2$	$C_{max}=3.782$ $\%S_{0,opt}=0.75$	$C_{max}=2.608$ $\%S_{0,opt}=0.75$	$C_{max}=2.108$ $\%S_{0,opt}=0.70$	$C_{max}=1.895$ $\%S_{0,opt}=0.65$
$Gr=10^4$	$\%D_0=0.05$	$C_{max}=2.921$ $\%S_{0,opt}=0.95$	$C_{max}=1.965$ $\%S_{0,opt}=0.90$	$C_{max}=1.588$ $\%S_{0,opt}=0.90$	$C_{max}=1.367$ $\%S_{0,opt}=0.90$
	$\%D_0=0.1$	$C_{max}=4.157$ $\%S_{0,opt}=0.90$	$C_{max}=2.771$ $\%S_{0,opt}=0.85$	$C_{max}=2.216$ $\%S_{0,opt}=0.85$	$C_{max}=1.896$ $\%S_{0,opt}=0.85$
	$\%D_0=0.2$	$C_{max}=5.760$ $\%S_{0,opt}=0.80$	$C_{max}=3.782$ $\%S_{0,opt}=0.75$	$C_{max}=3.035$ $\%S_{0,opt}=0.75$	$C_{max}=2.608$ $\%S_{0,opt}=0.75$

The values obtained for optimum two heat sources locations and the maximum overall heat transfer in different Richardson numbers 0.1, 1, 4 and 10, constant Grashof numbers 10^2, 10^3 and 10^4 and for three different heat source lengths are presented in Table 4. In all cases, the volume fraction is considered 0.05. In Figure 8, the maximum overall heat transfer in terms of the Grashof number is illustrated in constant Richardson number.

As a result, by increasing the Grashof number, heat transfer and the maximum overall heat transfer inside the cavity increases.

Augmentation intensity is greater for larger Grashof numbers.

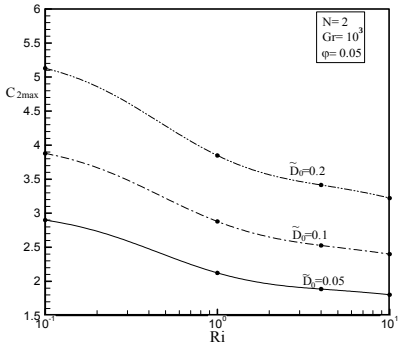

Fig. 7. Maximum overall heat transfer for different values of Richardson number and in $Gr=10^3$ and $\varphi=0.05$

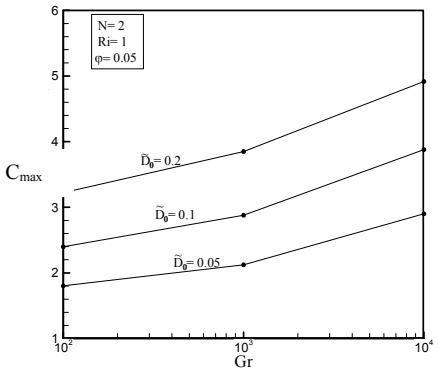

Fig. 8. Maximum overall heat transfer in terms of the Grashof number in constant Richardson number

As shown in Figure 8, by increasing the Grashof number, optimal heat sources location is migrated toward the ending corner of the left wall and the heat sources become close to each other. This subject is shown well in Table 5.

Table 5
Optimum heat source location ($\%S_{0.opt}$) and maximum overall heat transfer (C_{max}) for different Richardson numbers and constant Grashof numbers.

		Ri=0.1	**Ri=1**	**Ri=4**	**Ri=10**
$Gr=10^2$	$\%D_0$=0.05	C_{2max}=2.131 $\%S_{0,opt}$=0.65 $\%S_{1,opt}$=0.2	C_{2max}=1.803 $\%S_{0,opt}$=0.35 $\%S_{1,opt}$=0.4	C_{2max}=1.703 $\%S_{0,opt}$=0.25 $\%S_{1,opt}$=0.45	C_{2max}=1.677 $\%S_{0,opt}$=0.2 $\%S_{1,opt}$=0.45
	$\%D_0$=0.1	C_{2max}=2.879 $\%S_{0,opt}$=0.55 $\%S_{1,opt}$=0.2	C_{2max}=2.339 $\%S_{0,opt}$=0.3 $\%S_{1,opt}$=0.35	C_{2max}=2.259 $\%S_{0,opt}$=0.2 $\%S_{1,opt}$=0.4	C_{2max}=2.2 $\%S_{0,opt}$=0.2 $\%S_{1,opt}$=0.4
	$\%D_0$=0.2	C_{2max}=3.848 $\%S_{0,opt}$=0.4 $\%S_{1,opt}$=0.15	C_{2max}=3.222 $\%S_{0,opt}$=0.2 $\%S_{1,opt}$=0.3	C_{2max}=3.019 $\%S_{0,opt}$=0.15 $\%S_{1,opt}$=0.3	C_{2max}=2.929 $\%S_{0,opt}$=0.15 $\%S_{1,opt}$=0.3
$Gr=10^3$	$\%D_0$=0.05	C_{2max}=2.9 $\%S_{0,opt}$=0.75 $\%S_{1,opt}$=0.1	C_{2max}=2.133 $\%S_{0,opt}$=0.6 $\%S_{1,opt}$=0.25	C_{2max}=1.886 $\%S_{0,opt}$=0.45 $\%S_{1,opt}$=0.35	C_{2max}=1.803 $\%S_{0,opt}$=0.35 $\%S_{1,opt}$=0.4
	$\%D_0$=0.1	C_{2max}=3.879 $\%S_{0,opt}$=0.65 $\%S_{1,opt}$=0.1	C_{2max}=2.879 $\%S_{0,opt}$=0.55 $\%S_{1,opt}$=0.2	C_{2max}=2.527 $\%S_{0,opt}$=0.4 $\%S_{1,opt}$=0.3	C_{2max}=2.399 $\%S_{0,opt}$=0.3 $\%S_{1,opt}$=0.35
	$\%D_0$=0.2	C_{2max}=5.130 $\%S_{0,opt}$=0. 5 $\%S_{1,opt}$=0.1	C_{2max}=3.848 $\%S_{0,opt}$=0.4 $\%S_{1,opt}$=0.15	C_{2max}=3.415 $\%S_{0,opt}$=0.25 $\%S_{1,opt}$=0.25	C_{2max}=3.222 $\%S_{0,opt}$=0.2 $\%S_{1,opt}$=0.3
$Gr=10^4$	$\%D_0$=0.05	C_{2max}=4.167 $\%S_{0,opt}$=0. 85 $\%S_{1,opt}$=0.1	C_{2max}=2.9 $\%S_{0,opt}$=0. 75 $\%S_{1,opt}$=0.15	C_{2max}=2.315 $\%S_{0,opt}$=0. 7 $\%S_{1,opt}$=0.15	C_{2max}=2.133 $\%S_{0,opt}$=0. 6 $\%S_{1,opt}$=0.35
	$\%D_0$=0.1	C_{2max}=5.743 $\%S_{0,opt}$=0. 75 $\%S_{1,opt}$=0.5	C_{2max}=3.879 $\%S_{0,opt}$=0.65 $\%S_{1,opt}$=0.1	C_{2max}=2.948 $\%S_{0,opt}$=0. 55 $\%S_{1,opt}$=0.2	C_{2max}=2.680 $\%S_{0,opt}$=0. 55 $\%S_{1,opt}$=0.2
	$\%D_0$=0.2	C_{2max}=7.292 $\%S_{0,opt}$=0. 6 $\%S_{1,opt}$=0.0	C_{2max}=4.916 $\%S_{0,opt}$=0. 5 $\%S_{1,opt}$=0.1	C_{2max}=3.689 $\%S_{0,opt}$=0. 45 $\%S_{1,opt}$=0.1	C_{2max}=3.253 $\%S_{0,opt}$=0. 4 $\%S_{1,opt}$=0.15

According to Table 5, the maximum overall heat transfer for a heat source with length 0.5 and $Gr=10^3$ is C_{max}=1.367.

It is clear that with an increase of 100% heat source length, the maximum overall heat transfer only 38% increases and becomes C_{max}=1.896. The important aspect of the maximization of global performance is observed when the total heated area is held constant or in other words $N\widetilde{D_0} =$ cte.

Effect of the length and number of heat sources on overall heat transfer

Figure 9 shows Maximum overall heat transfer for $N\widetilde{D_0} =$ cte in different Richardson numbers and constant Grashof numbers 10^2 and 10^3.

In general and based on Figure 9, the maximum overall heat transfer increases in a regular pattern for different Richardson numbers while the number of heat sources increases in a fixed total length. This increasing is more for high Richardson numbers than low ones. But the striking thing is the difference in the augmentation intensity of maximum overall heat transfer for Grashof 10^2 and 10^3 in which by increasing the Grashof number, discrepancy between C_{2max} and C_{max} for $N\widetilde{D_0} = 0.1,0.2$ becomes less.

Figure 10 shows the overall heat transfer in terms of the Richardson numbers and in different volume fractions (0.01, 0.03, 0.05 and 0.09).

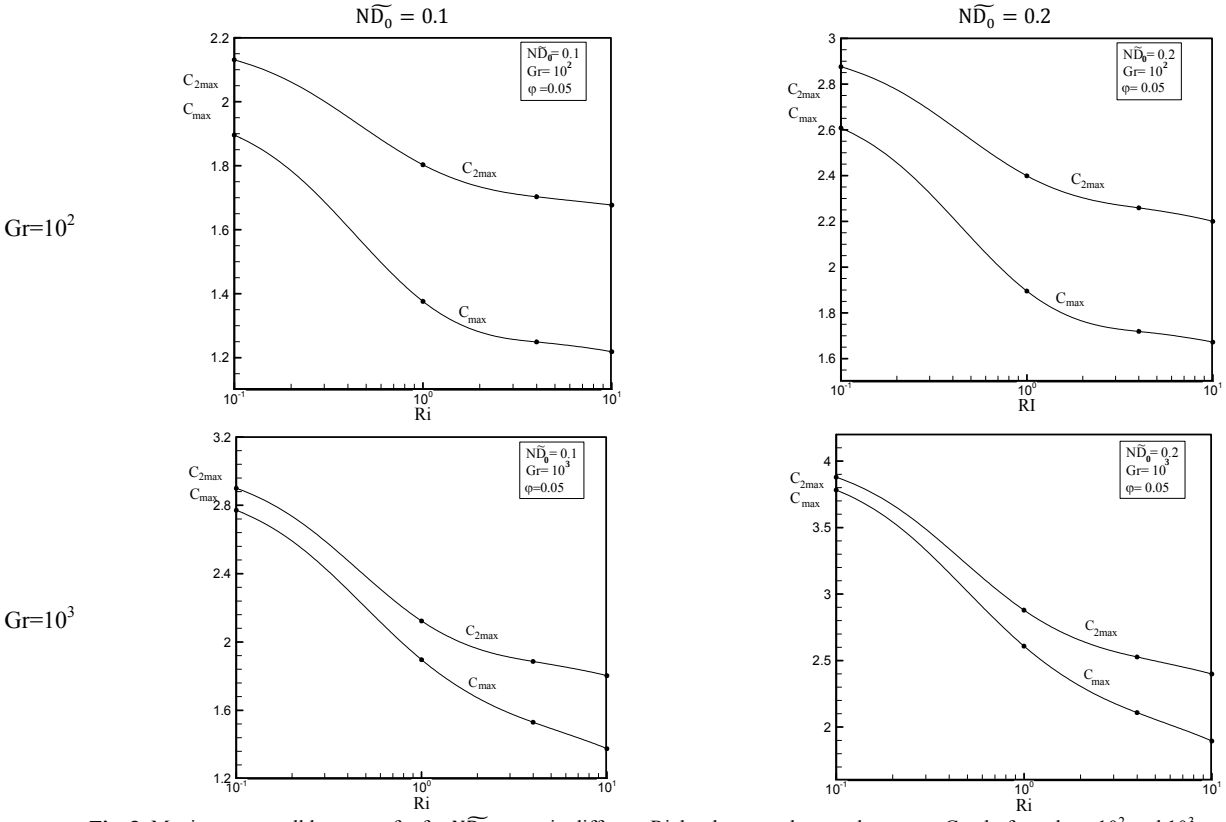

Fig. 9. Maximum overall heat transfer for $N\widetilde{D_0} =$ cte in different Richardson numbers and constant Grashof numbers 10^2 and 10^3

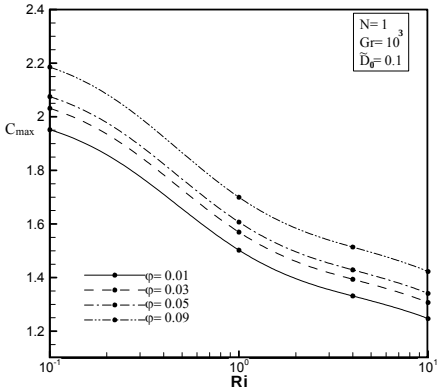

Fig. 10. Overall heat transfer Changes in different the volume fraction of nanoparticles

Constant heat source length is 0.1. As shown in this figure, heat transfer increases by increasing nanoparticles volume fractions and this increase is independent of the Richardson number.

Effect of the Richardson number and Grashof number on stream lines and isotherm

In Figures 11 and 12, stream lines and isothermal lines are depicted for constant nanoparticles volume fractions φ=0.05 and equal heat source length and location.

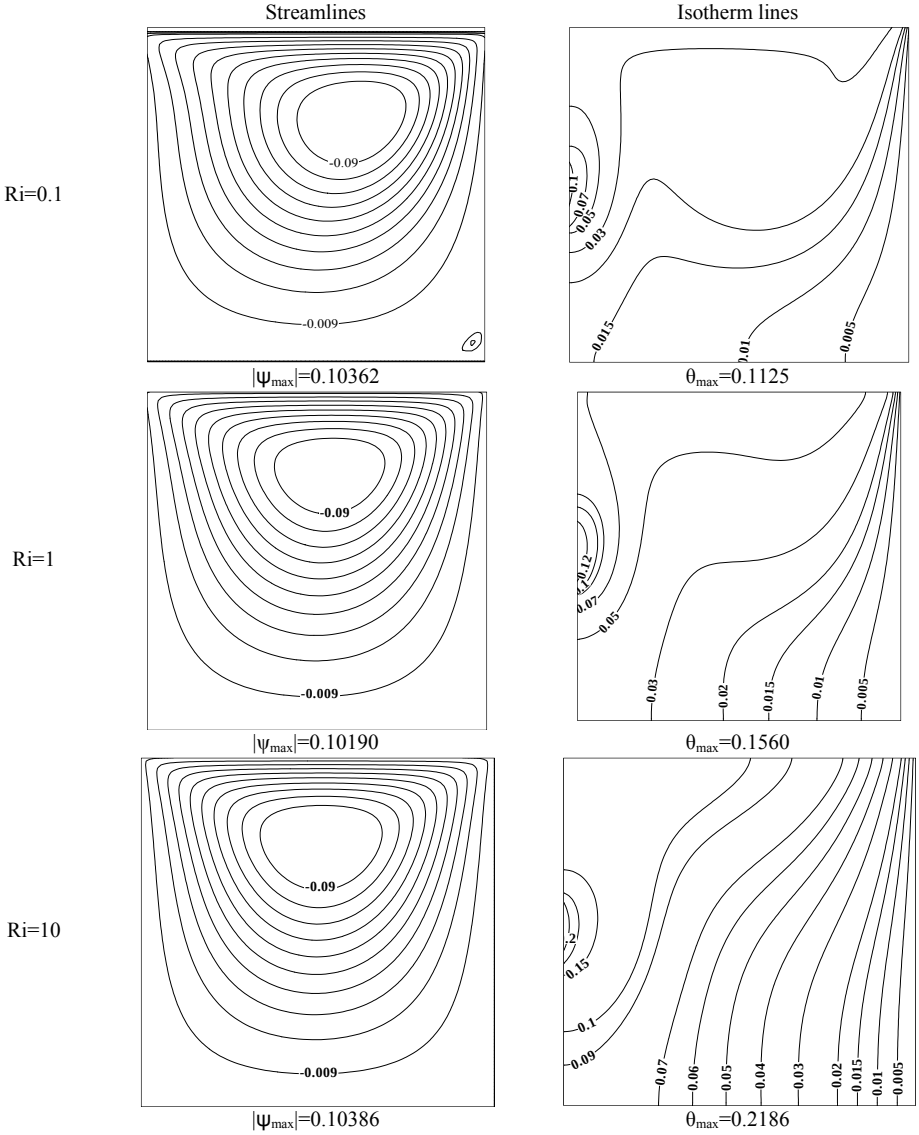

Fig. 11. Streamlines and isothermal lines in different values of Richardson number and in constant $Gr=10^2$

As illustrated in these figures, by reducing the Richardson number, vortex center moves toward the upper right corner and the lines agglomeration in this area increases and the small size counterclockwise vortex which is formed in the starting corner, becomes larger. Also by augmentation the Grashof number, vortex in the middle of the cavity becomes larger and transmits to the center of cavity. This subject represents an increase of fluid velocity near the walls. In addition by increasing the Grashof number, small counterclockwise vortices are formed in the bottom corner of the cavity in which the size of the vortices is larger on the right side of the cavity. Also stream lines density near the surfaces rise and thus the mass flow rate passing near the surface, increases. In $Gr=10^2$ and Ri=10 elements clockwise rotation is weak and the isothermal lines will become vertical. This issue represents the increasing of conduction heat transfer in the cavity. It should be noted that in general, by augmentation the Richardson number, isothermal lines with the same values approach to each other. Also when the Richardson number decreases, the

isothermal lines will be near to the horizontal state and the isothermal lines agglomeration besides the heat sources and cold wall increases. Thus the fluid which is in more contact to the walls causes enhancement in heat transfer and reduces the maximum heat source temperature.

By increasing the Grashof number due to strengthen of the buoyancy force, the stream function increases and the maximum temperature will be reduced.

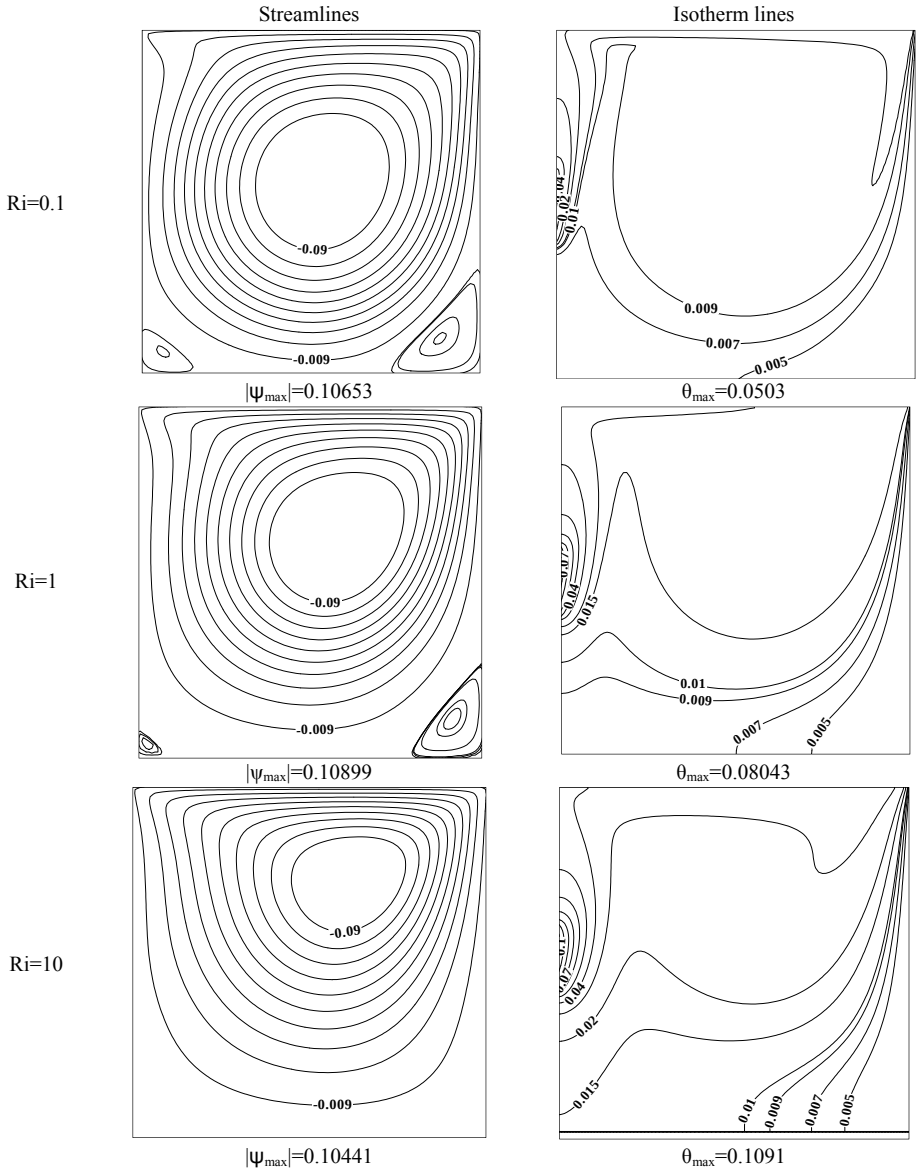

Fig. 12. Streamlines and isothermal lines in different values of Richardson number and in constant $Gr=10^4$.

Comparison of the average Nusselt number for two models of nanofluids

In this section the average Nusselt number compares for two different models; variable properties and constant properties. In the first case the properties of the water-Al_2O_3 varies with temperature, Khanafer and Vafai model [42] according to equations 10, 12 and 13 has been used. In the second case, the nanofluid properties are considered constant, Maxwell model [41] according to equation 11 and Brinkman model[48] according to equation 9 have been used.

As can be seen in Figure 13, in Maxwell and Brinkman models, by increasing the volume fraction, the average Nusselt number in a regular basis with constant slope increases but in Khanafer and Vafai model [42], the

average Nusselt number decreases by increasing the volume fraction. It is noteworthy that for both models, the average Nusselt number increases by decreasing the Richardson number which increases the heat transfer rate inside the cavity. For Ri=10, the average Nusselt numbers for the Khanafer and Vafai [42] model is less than Maxwell [41] and Brinkman [48] models and for Ri=0.1 this amount is greater. In Ri=1, the values which are obtained from these three models are almost equal but by increasing the volume fraction, the average Nusselt number in Maxwell [41] and Brinkman [48] model is less than Khanafer and Vafai [33] model.

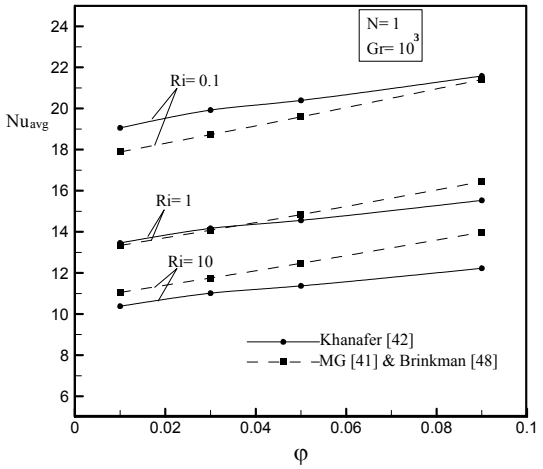

Fig. 13. Comparison of the average Nusselt number for constant properties model (Maxwell and Brinkman) and variable properties (Khanafer and Vafai model) in different Richardson numbers and nanoparticles volume fractions.

Conclusion

In the present study, the optimum heat sources locations with constant heat flux on the wall of a lid-driven square cavity containing water-Al_2O_3 nanofluids with variable properties are investigated numerically and the following results are obtained:

- When the Richardson number increases, the natural convection heat transfer become stronger, hence the optimal heat source location from the top wall moves to the midsection.
- In high Grashof numbers, range of optimum location is in upper part of the wall and near to the lid-driven that for different Richardson numbers, the optimal location change is negligible but in low Grashof number these changing are intensified and oriented toward the center of the wall.
- When the heat source is located on the bottom of the wall the overall heat transfer changes are very small for different Richardson numbers.
- By increasing nanoparticles volume fractions, the average Nusselt number on heat sources for both constant properties model (Maxwell and Brinkman) and variable properties (Khanafer and Vafai model) increases. The enhancement intensity for Maxwell and Brinkman model is constant but for Khanafer and Vafai model, decreases by increasing nanoparticles volume fraction.

References

[1] T. Basak, S. Roy, P.K. Sharma, I. Pop: Analysis of mixed convection flows within a square cavity with uniform and non-uniform heating of bottom wall, International Journal of Thermal Science 48 (2009) 891–912.

[2] G. Guo, M.A.R. Sharif: Mixed convection in rectangular cavities aspect ratios with moving isothermal sidewalls and constant flux heat source on the bottom wall, International Journal of Thermal Science 43 (2004) 465–475.

[3] A. Fattahi, M. Alizadeh: Numerical Investigation of Double- Diffusive Mixed Convective Flow in a Lid-Driven Enclosure Filled with Al2O3-Water Nanofluid, Transport Phenomena in Nano and Micro Scales 2 (2014) 65-77.

[4] A. Zare Ghadi, M. Sadegh Valipour: Numerical Study of Hydro-Magnetic Nanofluid Mixed Convection in a Square Lid-Driven Cavity Heated From Top and Cooled From Bottom, Transport Phenomena in Nano and Micro Scales 2 (2014) 29-42.

[5] B. Jafarian, M. Hajipour, R. Khademi: Conjugate Heat Transfer of MHD non-Darcy Mixed Convection Flow of a Nanofluid over a Vertical Slender Hollow Cylinder Embedded in Porous Media, Transport Phenomena in Nano and Micro Scales 4 (2016) 1-10.

[6] H. R. Ehteram, A. A. Abbasian Arani, G. A. Sheikhzadeh, A. Aghaei, A. R. Malihi: The effect of various conductivity and viscosity models considering Brownian motion on nanofluids mixed convection flow and heat transfer, Transport Phenomena in Nano and Micro Scales 4 (2016) 19-28.

[7] F. Vahidinia, M. Rahmdel: Turbulent Mixed Convection of a Nanofluid in a Horizontal Circular Tube with Non-Uniform Wall Heat Flux Using a Two-Phase Approach, Transport Phenomena in Nano and Micro Scales 3 (2015) 106-117.

[8] A. Aghaei, H. Khorasanizadeh, G. Sheikhzadeh, M. Abbaszadeh: Numerical study of magnetic field on mixed convection and entropy generation of nanofluid in a trapezoidal enclosure, Journal of Magnetism and Magnetic Materials 403 (2016) 133–145.

[9] A. Rahmati, A. R. Roknabadi, M. Abbaszadeh: Numerical simulation of mixed convection heat

transfer of nanofluid in a double lid-driven cavity using lattice Boltzmann method, Alexandria Engineering Journal Available online 20 September 2016, http://dx.doi.org/10.1016/j.aej.2016.08.017.

[10] M.A.R. Sharif: Laminar mixed convection in shallow inclined driven cavities with hot moving lid on top and cooled from bottom, Applied Thermal Engineering 27 (2007) 1036–1042.

[11] R.K. Tiwari, M.K. Das: Heat transfer augmentation in a two-sided lid-driven differentially heated square cavity utilizing nanofluids, International Journal Heat and Mass Transfer 50 (2007) 2002–2018.

[12] M. Muthtamilselvan, P. Kandaswamy, J. Lee: Heat transfer enhancement of Copper–water nanofluids in a lid-driven enclosure, Communications in Nonlinear Science Numerical Simulation 15 (2010) 1501–1510.

[13] A. Arefmanesh, M. Mahmoodi: Effects of uncertainties of viscosity models for Al_2O_3–water nanofluid on mixed convection numerical simulations, International Journal of Thermal Sciences 50 (2011) 1706–1719.

[14] P. Kandaswamy, S. Sivasankaran, N. Nithyadevi: Buoyancy-driven convection of water near its density maximum with partially active vertical walls, International Journal of Heat and Mass Transfer 50 (2007) 942-948.

[15] M. Mahmoodi: Mixed convection inside nanofluid filled rectangular enclosures with moving bottom wall, Thermal Science 15 (2011) 889–903.

[16] S. Mazrouei Sebdani, M. Mahmoodi, S.M. Hashemi: Effect of nanofluid variable properties on mixed convection in a square cavity, International Journal of Thermal Sciences 52 (2012) 112–126.

[17] A.M. Amiri, Kh.M. Khanafer, I. Pop: Numerical simulation of combined thermal and mass transport in a square lid-driven cavity, International Journal of Thermal Sciences 46 (2007) 662-671.

[18] A. Arefmanesh, A. Aghaei, H. Ehteram: Mixed convection heat transfer in a CuO–water filled trapezoidal enclosure, effects of various constant and variable properties of the nanofluid, Applied Mathematical Modelling 40 (2016) 815–831.

[19] A. Aghaei, GA. Sheikhzadeh, H. Ehteram, M. Hajiahmadi: Numerical Investigation of Mixed Convection Fluid Flow, Heat Transfer and Entropy Generation in Triangular Enclosure Filled with a Nanofluid, Journal of Applied Fluid Mechanics 9 (2016) 147-156.

[20] M. Najafi, M. Nikfar, A. Arefmanesh: Inclination angle implications for fluid flow and mixed convection in complex geometry enclosure-meshless numerical analyses, Journal of Theoretical and Applied Mechanics 53 (2015) 519-530.

[21] A. Saha, T. Malik: Mixed convection flow and heat transfer through a horizontal channel with surface mounted obstacles, Journal of Enhanced Heat Transfer 19 (2012) 313-329.

[22] S. H. Hussain, Q.R. Abd-Amer: Mixed convection heat transfer flow of air inside a sinusoidal corrugated cavity with a heat conducting horizontal circular cylinder, Journal of Enhanced Heat Transfer 18 (2011) 433-447.

[23] P. Shiang-Wuu, W. Horng-Wen: Heat transfer enhancement for turbulent mixed convection in reciprocating channel by various rib installation, Journal of Enhanced Heat Transfer 20 (2013) 95-114.

[24] T. Hayat, M. Bilal Ashraf, H.H. Alsulami: On mixed convection flow of Jeffrey fluid over an inclined stretching surface with thermal radiation, Heat Transfer Research 46 (2015) 515-539.

[25] M. Hemmat Esfe, A.H. Refahi, H. Teimouri, M.J. Noroozi, M. Afrand, A. Karimiopour: Mixed convection fluid flow and heat transfer of the Al2O3-water nanofluid with variable properties in a cavity with an inside quadrilateral obstacle, Heat Transfer Research 46 (2015) 465-482.

[26] M. Hemmat Esfe, M. Akbari, D.Toghraei Semiromi, A. Karimiopour, M. Afrand: Effect of nanofluid variable properties on mixed convection flow and heat transfer in an inclined two-sided lid-driven cavity with sinusoidal heating on side walls, Heat Transfer Research 45 (2014) 409-432.

[27] M. Hemmat Esfe, S.S. Mirtalebi Esforjani, M. Akbari, A. Karimiopour: Mixed-convection flow in a lid-driven square cavity with a nanofluid with variable properties: effect of the nanoparticle diameter and of the position of a hot obstacle, Heat Transfer Research 45 (2014) 563-578.

[28] S. Shehzad, F. E. Alsaadi, T. Hayat, S. J. Monaquel: MHD mixed convection flow of Thixo tropic fluid with thermal radiation, Heat Transfer Research 45 (2014) 569-676.

[29] M. Hemmat Esfe, S. Niazi, S.S. Mirtalebi Esforjani, M. Akbari: Mixed convection flow and heat transfer in a ventilated inclined cavity containing hot obstacles subjected to a nanofluid, Heat Transfer Research 45 (2014) 309-338.

[30] M. Hemmat Esfe, S.S. Mirtalebi Esforjani, M. Akbari: Mixed convection flow and heat transfer in a lid-driven cavity subjected to nanofluid: effect of temperature, concentration and cavity inclination angles, Heat Transfer Research 45 (2014) 453-470.

[31] F. Bazdadi-Tehrani, A. Safakish: Mixed-convection and thermal radiation heat transfer in a three dimensional asymmetrically heated vertical channel, Heat Transfer Research 45 (2014) 541-561.

[32] M. Mollamahdi, M. Abbaszadeh, G. Sheikhzadeh: Flow field and heat transfer in a channel with a permeable wall filled with Al_2O_3-Cu/water micropolar hybrid nanofluid, effects of chemical reaction and magnetic field, Journal of Heat and

Mass Transfer Research Available online from 2 September 2016.

[33] M. Abbaszadeh, A. Ababaei, A. A. Abbasian Arani, A. Abbasi Sharifabadi: MHD forced convection and entropy generation of CuO‐water nanofluid in a microchannel considering slip velocity and temperature jump, The Brazilian Society of Mechanical Sciences and Engineering First Online: 7 June 2016, DOI 10.1007/s40430-016-0578-7.

[34] G. Sheikhzadeh, A. Aghaei, H. Ehteram, M. Abbaszadeh: Analytical study of parameters affecting entropy generation of nanofluid turbulent flow in channel and micro-channel, Thermal Science (2016) Online-First Issue, DOI: 10.2298/TSCI151112070S.

[35] G.A. Sheikhzadeh, H. Khorasanizadeh, S.P. Ghaffari: Mixed Convection of Variable Properties Al2O3-EG-Water Nanofluid in a Two-Dimensional Lid-Driven Enclosure, Transport Phenomena in Nano and Micro Scales 1 (2013) 75-92.

[36] G. A. Sheikhzadeh, H. Teimouri, M. Mahmoodi: Numerical Study of Mixed Convection of Nanofluid in a Concentric Annulus with Rotating Inner Cylinder, Transport Phenomena in Nano and Micro Scales 1 (2013) 26-36.

[37] A. Muftuoglu, E. Bilgen: Conjugate heat transfer in open cavities with a discrete heater at its optimized position, International Journal of Heat and Mass Transfer 51 (2007) 779-788.

[38] Y. Liu, N.P. Thien: An optimum placing problem for three chips mounted on a vertical substrate in an enclosure, Numerical Heat Transfer Part A 37 (2000) 613–630.

[39] S. Chen, Y. Liu, S.F. Chan, C.W. Leung, T.L. Chan: Experimental study of optimum spacing in the cooling of simulated electronic package, Heat and Mass Transfer 37 (2001) 251–257.

[40] Tito Dias Jr., L.F. Milanez: Optimal location of heat sources on a vertical wall with natural convection and genetic algorithm, International Journal of Heat and Mass Transfer 49 (2006) 2090–2096.

[41] J.C. Maxwell, A Treatise on Electricity and magnetism, second ed., clarendon press, Oxford, UK. (1881).

[42] Kh. Khanafer, K, Vafai: A critical synthesis of thermophysical characteristics of nanofluids, International journal of heat and mass transfer 54 (2011) 4410-4428.

[43] A. Bejan, Convection Heat Transfer. John Wiley & Sons, Inc., Hoboken, New Jersey, USA, 2004.

[44] G. Sheikhzadeh, H. Ghasemi, M. Abbaszadeh: Investigation of natural convection boundary layer heat and mass transfer of MHD water-AL2O3 nanofluid in a porous medium, International Journal of Nano Studies & Technology (IJNST) 5 (2) 110-122.

[45] K. Khanafer, K. Vafai, M. Lightstone: Buoyancy-driven heat transfer enhancement in a two-dimensional enclosure utilizing nanofluid, International journal of heat and mass transfer 46 (2003) 3639-3653.

[46] A.K. da Silva, S. Lorente, A. Bejan: Optimal distribution of discrete heat sources on a wall with natural convection, International journal of heat and mass transfer 47 (2004) 203-214.

[47] V. Sivakumar, S. Sivasankaran, P. Prakash, Jinho lee: Effect of heating and size on mixed convection in lid-driven cavities, Computers and Mathematics With Application 59 (2010) 3053-3065.

[48] H.C. Brinkman: The viscosity of concentrated suspensions and solutions, The Journal of Chemical Physic 20 (1952) 571.